MOLECULAR PHYSICS, 2002, VOL. 100, NO. 23, 3711–3721

Taylor & Francis
Taylor & Francis Group

Molecular orbital study of polarity and hydrogen bonding effects on the g and hyperfine tensors of site directed NO spin labelled bacteriorhodopsin

MARTIN PLATO[1], HEINZ-JÜRGEN STEINHOFF[2], CHRISTOPH WEGENER[2], JENS T. TÖRRING[1], ANTON SAVITSKY[1] and KLAUS MÖBIUS[1]*

[1] Institut für Experimentalphysik, Freie Universität, Arnimallee 14, 14195 Berlin, Germany

[2] Fachbereich Physik, Universität Osnabrück, Barbarastrasse 7, 49069 Osnabrück, Germany

Semiempirical molecular orbital methods (PM3, INDO, ZINDO/S) have been used to calculate the effects of local electric fields and of hydrogen bonding on the g and hyperfine tensors of a nitroxide spin label model system. The results yield a linear correlation between the two principal tensor components g_{xx} and A^{N}_{zz} at label sites of varying polarity. Hydrogen bonding with a single water molecule produces a constant shift of $\Delta g_{xx} \cong -4 \times 10^{-4}$. These theoretical results are used to interpret recent high field (3.4 T, 95 GHz) electron paramagnetic resonance investigations on site-directed spin labelled bacteriorhodopsin. This protein reveals a close correlation between proticity and polarity at the various label sites. The slope of the g_{xx} versus A^{N}_{zz} dependence is affected strongly by polarity induced structural strains of the spin label.

1. Introduction

This quantum mechanical molecular orbital (MO) study was instigated by high field electron paramagnetic resonance (EPR) investigations of the structure and conformational changes of site-directed spin labelled bacteriorhodopsin (BR) [1, 2]. The enhanced Zeeman splitting in these high field EPR spectra, obtained at 95 GHz and 3.4×10^4G = 3.4T, gave resolved g and ^{14}N hyperfine tensor components of the nitroxide (NO) spin label, g_{ii} and A^{N}_{ii}, respectively. The tensor element g_{xx}, in particular, shows significant variations with the NO label position in BR. These result from changes in the polarity of the label environment (polar effects) and/or from the varying availability of protons for hydrogen bond formation with the NO label (protic effects). Thus, the tensor element g_{xx} may be used to characterize the hydrophobic barrier ions have to overcome during their paths through possible ion channels.

When plotting g_{xx} against A^{N}_{zz} for 13 different spin label sites, these show a close grouping around a straight line connecting two prominent points A and B, as shown in figure 1. Point A is characterized by a practically nonpolar and aprotic label microenvironment, while B corresponds to a strongly polar and protic situation. These points have been approximated experimentally by the free (rigid) label in toluene/polystyrene and in pure water, respectively. Point A was not included in the results of [1, 2] and has been added in the later course of these investigations. The results of [1], presented in figure 3B therein, are reinterpreted in the present theoretical study as a consequence of this additional piece of information. However, all qualitative arguments in [1, 2] remain valid.

It is the goal of the present MO theoretical study to obtain a semiquantitative description of the g_{xx} versus A^{N}_{zz} behaviour in NO spin label environments of different physical and/or chemical nature. It covers solute–solvent interactions such as matrix polarity as well as hydrogen bonding (hb). These two types of interaction are superimposed, thus defining the range between the aprotic (no hb) and protic (partial to large scale hb) limits.

One of the aims of this study is to extract a measure for the protic contribution from the observed g_{xx} versus A^{N}_{zz}. Such protic effects are of particular interest in studies of site directed spin labelled proteins as they help to characterize the accessibility of putative ion channels for water and the proton mobility in the channels of different protein moieties [1, 2]. An important

* Author for correspondence. e-mail: moebius@physik.fu-berlin.de

Molecular Physics ISSN 0026–8976 print/ISSN 1362–3028 online
http://www.tandf.co.uk/journals
DOI: 10.1080/0026897021016624 6

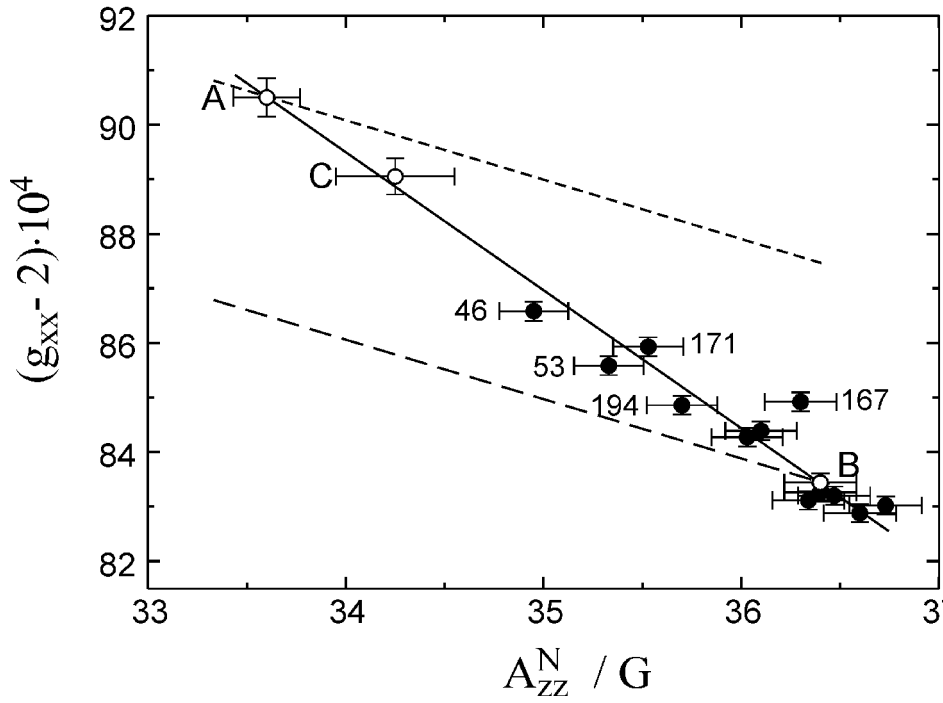

Figure 1. Plot of g_{xx} versus A^N_{zz} for various spin label positions in BR [1, 2]. The plot includes values measured for the free rigid label in toluene/polystyrene (point A) and in water (point B). Point C marks the results found for the triple mutant D96G/F171R1/F219L [2]. Horizontal and vertical bars indicate 2σ experimental errors. The dashed lines define the limits between the non-hydrogen bonded (short dashed) and fully hydrogen bonded (long dashed) cases. They were derived in analogy with the corresponding theoretical lines in figure 6 (*vide infra*).

additional aspect in site directed spin label studies is possible structural changes of the NO label itself, induced by the electrostatic field of the environment ('polarity induced strain'). Obviously, the assessment of such effects is important to discriminate between probe characteristics and matrix properties. Such structural changes of the label itself are studied in some detail in the context of the g_{xx} versus A^N_{zz} 'slope problem', which arises when trying to reproduce theoretically the observed slope of the linear dependence of g_{xx} or A^N_{zz}.

All MO calculations in this study are performed at a semiempirical level of the PM3, INDO and ZINDO/S type [3]. This approach is considered sufficient for a semiquantitative understanding of the various polar and protic effects on spin labels in proteins. It has also been taken by Un *et al.* [4], Törring *et al.* [5] and Knüpling *et al.* [6] for g tensor calculations on tyrosyl radicals in proteins, on semiquinone radical anions in solvents of varying polarity and on a series of organic radicals, respectively.

The effects of hydrogen bonding on the g tensor of NO spin labels were investigated by Engström *et al.* [7] using a restricted open-shell Hartree–Fock (ROHF) linear response method with the atomic mean field approximation (AMFI) [7]. These authors arrived at essentially the same results as found in the present study. This investigation [7] was followed by an EPR study by the same group on the MTS spin label (see below) in various solvents, including density functional theory (DFT) calculations of the g and N hyperfine tensors [8]. These latter calculations were performed for varying dielectric constants of the solvent medium and for a varying number of hydrogen bonds formed with the oxygen atom of the NO bond. However these two investigations [7, 8] do not directly aim at the interpretation of the g_{xx} versus A^N_{zz} found in site directed spin labelled BR [1, 2].

After completion of this manuscript, we became aware of a very recent study by Gullá *et al.* [9] of the effects of local electric fields E_{loc} on the g tensor of two ionized spin probes. These measurements allow a direct calibration of the observed g shifts with respect to E_{loc}, thus providing a means of determining the magnitude and direction of local electric fields. A comparison of those findings with our theoretical results on g_{ii} versus E_{loc} will be presented in the discussion.

2. Computational methods

2.1. *Structure of model NO spin label*

All computations have been restricted to the model NO spin label shown in figure 2 and abbreviated by NO1 in this paper. This compound is a close chemical model of the 'probe head' of the MTS ((1-oxil-2,2,5,5-tetramethylpyrroline-3methyl)methanesulphonate) spin label also shown in figure 2. This label was used in [1, 2], which are our principal experimental reference papers (section 1).

The geometry of NO1 was optimized at the semiempirical PM3 and INDO levels using the PC based molecular modelling package Hyperchem for WIN-

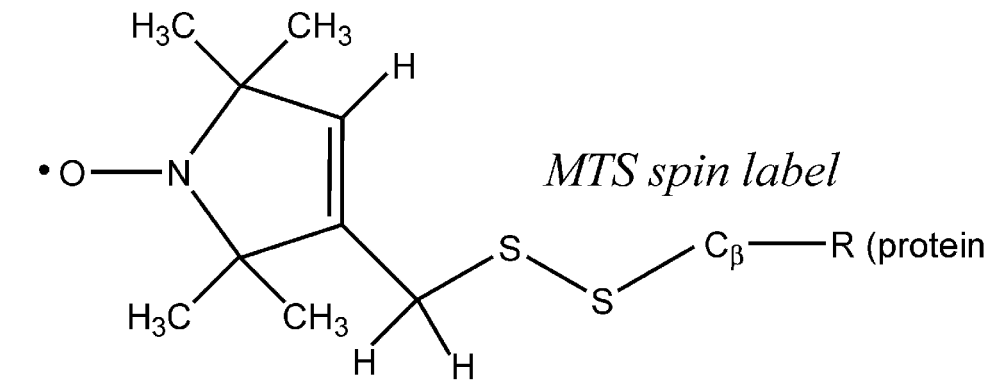

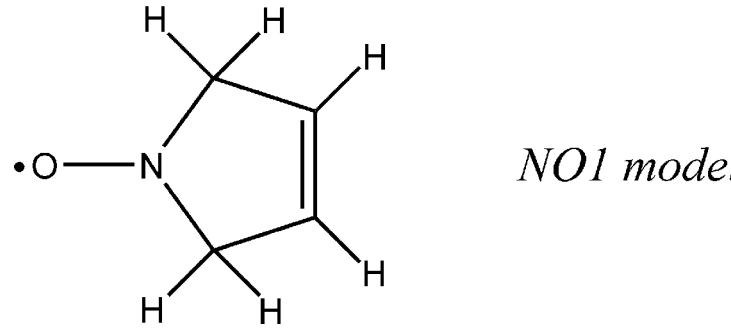

Figure 2. Molecular structures of the NO spin label MTS used in BR[1] and of the model NO spin label NO1.

DOWS™, distributed by Hypercube Inc., Gainsville, FL 32601, USA (Professional Release 6). Only the results for the PM3 geometry optimization will be presented in detail; however, we shall point out also major differences in the corresponding INDO results.

PM3 and INDO geometry optimizations of NO1 both yield a planar structure for the heavy atom skeleton (figure 2). This is in accordance with the X-ray structural analysis of compounds of the type NO1 with five-membered rings [10]. We postulate this structural feature as property of the 'free' unstrained NO1 in a non-polar microenvironment. However, we shall allow for certain deviations from this planar structure in polar microenvironments (see section 3.3 for details).

2.2. *Polarity effects*

Polarity effects from the various intermolecular fields in the non-bonding case are described by a single collective parameter: the average local electric field E in the NO bond region. This approach was first taken by Griffith *et al.* [11] in order to avoid the formidable task of a precise treatment of all individual contributions, e.g., dispersion forces, permanent electric dipole interactions, induced dipole interactions. As an example, these authors showed by first-order perturbation theory in the Hückel molecular orbital (HMO) frame that the π spin density at the nitrogen atom ρ_π^N increases to first order as

$$\Delta\rho_\pi^N = C_1 E_x \qquad (C_1 > 0), \tag{1}$$

where E_x is the electric field component along the NO bond (figure 3). The reason for this inherent

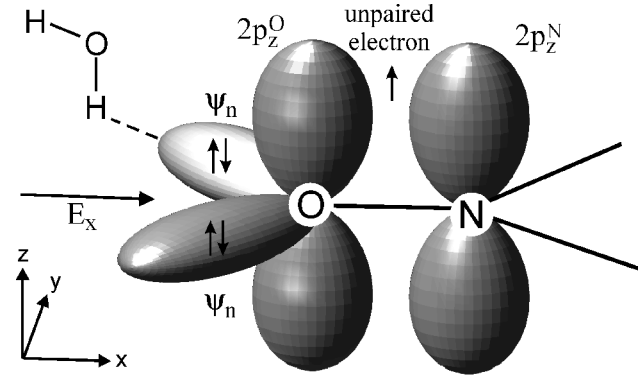

Figure 3. Electronic structure (schematic) of the NO bond with an external electric field arising from surrounding polar regions and with hydrogen bond formation. The non-bonding lone pair orbitals ψ_n are a superposition of oxygen 2s, 2p$_x$ and 2p$_y$ orbitals: $\psi_n = c_{ns}(2s) + c_{nx}(2p_x) + c_{ny}(2p_y)$.

orientational selectivity is the permanent electric dipole of the NO label pointing along the NO bond direction (conventionally defined as x direction). We have adopted this concept for studying polarity effects on the various molecular quantities determining the molecular g tensor and the nitrogen hyperfine tensor (see sections 2.4 and 2.5).

An estimate of C_1 in equation (1) on the basis of HMO theory yields a value of the order of $2 \times 10^{-9}\,\mathrm{V}^{-1}\,\mathrm{cm}$ [11]. The observed maximum change in the dipolar hyperfine component A_{zz} of the nitrogen atom is of the order of 8%, thus yielding $\Delta\rho_\pi^{\mathrm{N}} \lesssim 0.04$ for $\rho_\pi^{\mathrm{N}} \cong 0.5$. This gives $E_x \lesssim 2 \times 10^7\,\mathrm{V\,cm^{-1}}$ as a coarse estimate. In our calculations we consider variations of E_x between 0 and $10^8\,\mathrm{V\,cm^{-1}} \cong 0.02$ atomic units (au) ($1\,\mathrm{au} = 5.14 \times 10^9\,\mathrm{V\,cm^{-1}} = 51.4\,\mathrm{V\AA^{-1}}$).

The required local electric field E_x may be created in the algorithm of the Hyperchem molecular modelling package either by placing appropriate electric charges on the x axis in the near vicinity of the NO bond or by superimposing a homogeneous electric field parallel to the x axis. Since nearby electric charges produce inhomogeneous electric fields and would require the introduction of an additional parameter, we prefer the homogeneous field option. However, the results for one inhomogeneous case will also be presented for discussion.

2.3. *Hydrogen bonding*

Effects of hydrogen bonding (hb) have been studied on energy minimized structures of NO1 with *one* water molecule bound to the O atom ($\mathrm{NO1} + 1\mathrm{H_2O}$), see figure 3. There appears to be a high uncertainty in the literature concerning the number of hydrogen bonds formed with NO labels in aqueous solutions [8]. Statistically, this number may range between 0 and 2. From calculations of g tensor components and spin densities of MTS spin labels [7], we conclude that the formation of *two* hydrogen bonds ($\mathrm{NO1} + 2\mathrm{H_2O}$) is simply *additive* in its effects on g_{xx} and A_{zz}^{N}.

The PM3 method used for the geometry optimization of the combined molecules NO1 + $1\mathrm{H_2O}$ has been shown to describe hydrogen bond interactions the most accurately of all standard semiempirical methods [12]. The same approach was taken by Un *et al.* [4] in a theoretical g tensor study on tyrosyl radicals, specifically on a *p*-methylphenoxy radical/acetic acid molecular pair. Since hb effects are superimposed on purely electrostatic polarity effects, geometry optimization on $\mathrm{NO1} + 1\mathrm{H_2O}$ was performed at different values of the local electric field E_x.

2.4. *The* g *tensor*

The theory of g tensors of organic radicals was first developed by Stone [13]. The dominant contribution to the in-plane g tensor components of interest, g_{xx} and g_{yy}, arises from the spin–orbit coupling. The spin–orbit interaction couples the singly occupied ground state molecular orbital or SOMO (given the index 0) to an excited state SOMO (index i) and modifies the electron g value according to

$$g_{rt} = g_{\mathrm{e}}\delta_{rt} - 2\sum_{i\neq 0}\frac{\langle\Psi_0|\zeta(r)L_r|\Psi_i\rangle\langle\Psi_i|L_t|\Psi_0\rangle}{E_i - E_0}, \qquad (2)$$

where $g_{\mathrm{e}} = 2.002\,322$ is the free electron g value; Ψ_0, Ψ_i are the ground and excited SOMO states, respectively, E_0, E_i are the respective state energies, $\zeta(r)$ is the spin–orbit coupling function, and $L_r, L_t (r, t = x, y, z)$ are the orbital angular momentum operators. Stone proposed replacing the energy denominator $E_i - E_0$ by the difference $\varepsilon i - \varepsilon_0$ of the corresponding orbital energies. This is a rather drastic approximation since it neglects differences in exchange and Coulomb interactions between the ground and excited states. By contrast, we have explicitly used electronic state energies within the restricted Hartree–Fock (RHF) 'half-electron' approximation, where

$$E_i - E_0 = \pm(\varepsilon i - \varepsilon_0) - J_{i0} + 0.5K_{i0} + 0.5J_{00} \qquad (3)$$

and the + or − sign holds for the one-electron excitations $0 \rightarrow i$ or $i \rightarrow 0$, respectively [14].

In equation (3), J and K describe the Coulomb and exchange interactions between the denoted states. For the unoccupied orbitals $i > 0$, J and K are calculated using the corresponding virtual ground state MOs.

All the quantities needed for calculating g_{rt} by equations (2) and (3) are computed at the semiempirical ZINDO/S level from RHF ground state MOs (without configuration interaction). This option is also available within the Hyperchem molecular modelling package. ZINDO/S has been parametrized by Zerner *et al.* [15] to give satisfactory excitation energies $E_i - E_0$ for the interpretation of optical spectra. For this reason, we have analogously termed our computational approach the G-RHF/S method.

A similar approach with regard to the evaluation of the energy denominator in equation (2) has been taken by Hsiao *et al.* [16] in calculating the g tensors of several organic radicals. However, these authors use the restricted open shell variant ROHF of the ZINDO/S method, which performs very similarly to our 'half-electron' approach. Furthermore we have used the G-RHF/S

method at two levels of approximation with regard to the evaluation of matrix elements in equation (2).

2.4.1. *Approximation 1, G-RHF/S1*

Following the conventional LCAO-ansatz for molecular orbitals, only one-centre terms over atomic orbitals are retained in the matrix elements of equation (2). This is a basic assumption in the *g* factor theory of Stone [13], but only weakly justifiable, particularly for matrix elements not containing the spin–orbit coupling function $\zeta^{(r)}$ with its cutoff property [14].

2.4.2. *Approximation 2, G-RHF/S2*

Matrix elements in equation (2) not containing ζ are calculated including all 2- and 3-centre contributions. These have been derived analytically for Slater orbitals by Törring *et al.* [14].

The following spin–orbit coupling parameters for p electrons have been used in the *g* tensor calculations: $\zeta(\mathrm{C}) = 28, \zeta(\mathrm{N}) = 76, \zeta(\mathrm{O}) = 151\ \mathrm{cm}^{-1}$ [17].

2.4.3. *A simplified approach*

In order to assist the discussion of the computational results, we also make use of a simple model describing the essential contributions to the *g* tensor of an NO spin label, which has been used widely in the literature [18]. The major contributions to g_{rt} are derivable from a simplified schematic view of the electronic structure of the NO bond as depicted in figure 3. To a first approximation, g_{rt} is given by [18]

$$\begin{aligned} g_{xx} &\approx g_e + 2\zeta(\mathrm{O})\rho_\pi^{\mathrm{O}} c_{\mathrm{n}y}^2/\Delta E_{\mathrm{n}\to\pi}, \\ g_{yy} &\approx g_e + 2\zeta(\mathrm{O})\rho_\pi^{\mathrm{O}} c_{\mathrm{n}x}^2/\Delta E_{\mathrm{n}\to\pi}, \\ g_{zz} &\approx g_e, \\ g_{rt} &= 0 \qquad \text{for } r \neq t \qquad r, t = x, y, z, \end{aligned} \tag{4}$$

where ρ_π^{O} is the π spin density c_{somo}^2 on the oxygen $2p_z$ atomic orbital; $c_{\mathrm{n}x}$, $c_{\mathrm{n}y}$ are the MO coefficients of the $2p_x$ and $2p_y$ atomic orbitals contributing to the oxygen lone pair orbital Ψ_{n} (briefly n), and $\Delta E_{\mathrm{n}\to\pi}$ is the $\mathrm{n} \to \pi$ excitation energy. Equation (4) may be justified by the fact that the lone pair orbital n lies energetically very close to the lowest half-filled π orbital (ground state SOMO). All variable quantities in equation (4) will be extracted from the general RHF-ZINDO/S results and partly presented graphically as a function of the polarity parameter E_x (see section 3.2.1).

2.5. *The nitrogen dipolar hyperfine tensor A^N*

The dominant ^{14}N hyperfine splitting in the EPR spectra of immobile NO spin labels is observed along the principal *z* axis of the *g* tensor. This axis coincides with the molecular *z* axis (figure 3), ignoring minor deviations for the hb or non-planar cases. Therefore we have to compute A_{zz}^{N}, which separates into an isotropic term $a_{\mathrm{iso}}^{\mathrm{N}}$, arising from π–σ spin polarization of the inner nitrogen s shells (Fermi contact interaction) and into an anisotropic term $A_{\mathrm{dip},zz}^{\mathrm{N}}$, arising from the magnetic dipolar interaction between the delocalized unpaired electron and the N nucleus:

$$A_{zz}^{\mathrm{N}} = a_{\mathrm{iso}}^{\mathrm{N}} + A_{\mathrm{dip},zz}^{\mathrm{N}}. \tag{5}$$

It has been shown by Lemaire *et al.* [19] that $a_{\mathrm{iso}}^{\mathrm{N}}$ is practically independent of the π spin density on the neighbouring O atom, and thus is directly proportional to the π spin density ρ_π^{N} in the $2p_z^{\mathrm{N}}$ orbital. However, $a_{\mathrm{iso}}^{\mathrm{N}}$ also may partially contain 'direct' hyperconjugative contributions $\rho_{\mathrm{s}}^{\mathrm{N}}$ from the $2s^{\mathrm{N}}$ orbital in non-planar NO systems where the sp^2–p_z hybridization of the N atom is perturbed. Thus, more generally,

$$a_{\mathrm{iso}}^{\mathrm{N}} = Q_{\pi-\sigma}^{\mathrm{N}}\rho_\pi^{\mathrm{N}} + Q_{\mathrm{s}}^{\mathrm{N}}\rho_{\mathrm{s}}^{\mathrm{N}} \tag{6}$$

On the other hand, $A_{\mathrm{dip},zz}^{\mathrm{N}}$ is entirely determined by ρ_π^{N}, again with a vanishingly small contribution from ρ_π^{O}. This conclusion follows from an estimate of $\partial A_{\mathrm{dip},zz}^{\mathrm{N}}/\partial\rho_\pi^{\mathrm{O}} \approx -1$ MHz for $r_{\mathrm{NO}} = 1.3$ Å using formulae derived by Beveridge *et al.* [20] for 2p Slater orbitals and by comparing this with $\partial A_{zz}^{\mathrm{N}}/\partial\rho_\pi^{\mathrm{N}} \approx 73\ \mathrm{G} = 204$ MHz (equation (8)). Thus

$$A_{zz}^{\mathrm{N}} = Q_{\mathrm{tot}}^{\mathrm{N}}\rho_\pi^{\mathrm{N}} + Q_{\mathrm{s}}^{\mathrm{N}}\rho_{\mathrm{s}}^{\mathrm{N}}. \tag{7}$$

We use

$$Q_{\mathrm{tot}}^{\mathrm{N}} = 73\ \mathrm{G}$$

and

$$Q_{\mathrm{s}}^{\mathrm{N}} = 232\ \mathrm{G}. \tag{8}$$

The value for $Q_{\mathrm{tot}}^{\mathrm{N}}$ is adjusted to the value of $A_{zz}^{\mathrm{N}} = 33.6$ G observed for the MTS spin label in a non-polar environment (toluene/polystyrene), where we assume a planar structure with $\rho_{\mathrm{s}}^{\mathrm{N}} = 0$, and where $\rho_\pi^{\mathrm{N}} = 0.46$ from the ZINDO/S calculations (see section 3). The value for $Q_{\mathrm{s}}^{\mathrm{N}}$ is adopted from earlier INDO/S studies [21].

3. Results and discussion

3.1. *Structural details*

3.1.1. *Free planar NO1*

The NO bond length r_{NO} of the PM3 energy minimized structure varies between $r_{\mathrm{NO}} = 1.247$ Å (INDO: 1.247 Å) for $E_x = 0$ and $r_{\mathrm{NO}} = 1.269$ Å (INDO: 1.250 Å) for $E_x = 0.02$ au. Comparable X-ray values are around 1.27 ± 0.01 Å [10]. The increase in r_{NO} with E_x is accompanied by a significant increase in the electric

dipole moment from 5 D to 7 D (ZINDO/S). Not unexpectedly, in the free label the NO bond (molecular x axis) aligns along the electric field. There is no translational force acting on the label in a homogeneous electric field because of the vanishing total charge. In the planar structure, the N atom is $2sp^2_{x,y}$–p_z hybridized with a calculated CNC bond angle of 109° (110°) and with zero spin density in the σ orbitals 2s, $2p_x$ and $2p_y$ at the RHF-ZINDO/S level. X-ray analysis yields a CNC angle of 115° [10].

3.1.2. *Hydrogen bonded planar NO1*

The PM3 geometry optimization converges to an NO1 + $1H_2O$ structure in which the HOH plane of the water molecule settles about 0.3 Å above the xy plane of NO1 (figure 3). The H···O bond length varies weakly with E_x, ranging between 1.81 Å ($E_x = 0$) and 1.77 Å ($E_x = 0.02$ au). This corresponds to a moderately strong hydrogen bond with predominant electrostatic character [22]. The angle H···O—N is calculated to be around 122 ± 7°, being only weakly dependent on E_x. Therefore the H···O bond is roughly aligned along one of the lone pair orbital lobes with predominant $2p_y$ character, as would be expected (figure 3).

3.2. *The g and ^{14}N hyperfine tensors*

3.2.1. *The quantities ρ_π^O, c^2_{ny}, $\Delta E_{n\to\pi}$ and ρ_π^N*

Figure 4 presents an overview of the polarity dependence of the various molecular quantities governing the two tensors, g and A^N, as calculated by the RHF-ZINDO/S method. The plot contains the quantities ρ_π^O, c^2_{ny}, $\Delta E_{n\to\pi}$, and ρ_π^N introduced in equations (4) and (6), with and without hydrogen bonding (hb). We have omitted c^2_{nx} since the associated g tensor component g_{yy} is only very weakly dependent on E_x, and therefore has not been rigorously measured (calculated values for g_{yy} will, however, be given further down in the text).

A particularly critical quantity for the theoretical analysis is the excitation energy $\Delta E_{n\to\pi}$. We have

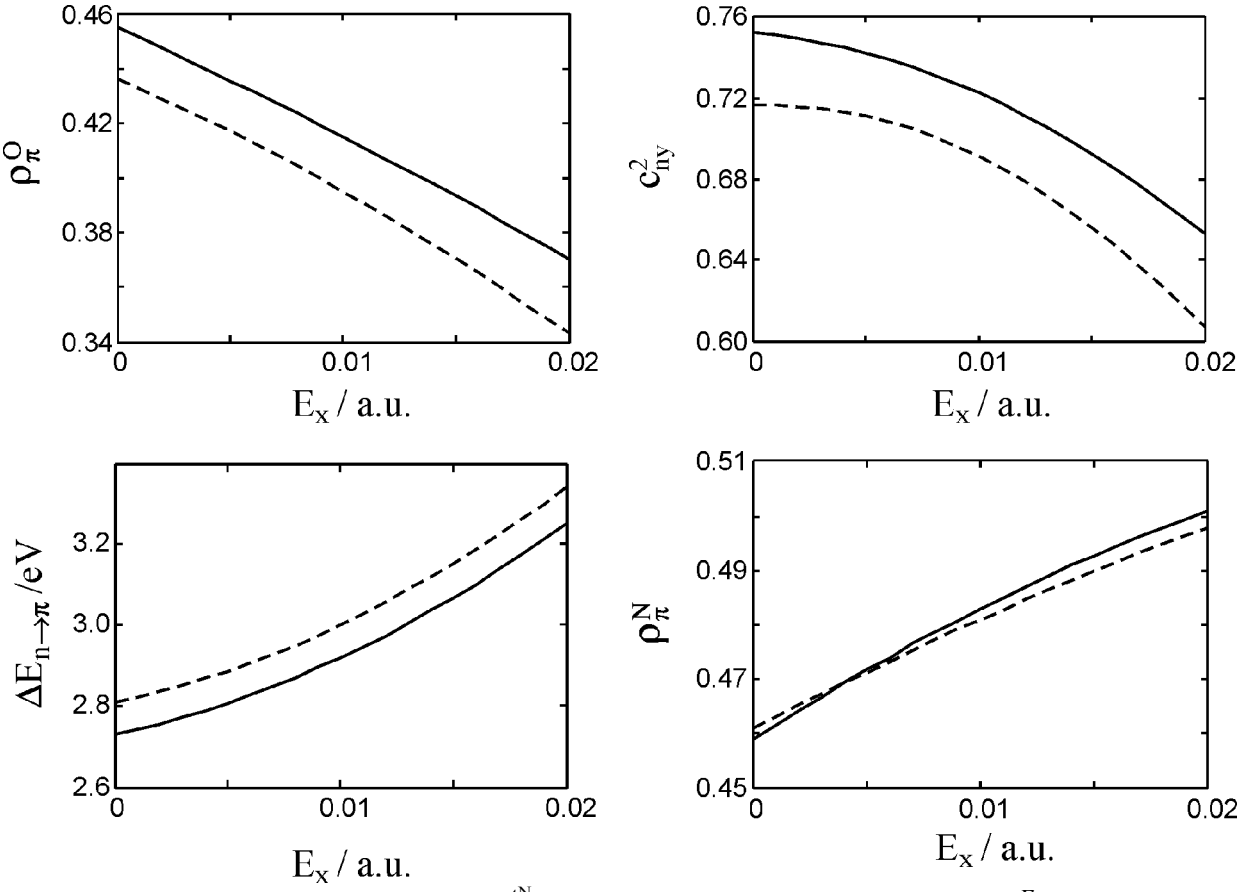

Figure 4. Molecular properties controlling the g and A^N tensors as a function of the polarity parameter E_x defined in the text. The NO1 structure is optimized by PM3. ρ_π^O is the oxygen π spin density, c^2_{ny} is the lone pair electron density of orbital component $2p_y^O$ (highest filled n orbital only, figure 2), $\Delta E_{n\to\pi}$ is the energy of electronic excitation n → π, and ρ_π^N is the nitrogen π spin density. The dashed lines are with hydrogen bond formation on the PM3 optimized NO1 + $1H_2O$ structure (see text).

adjusted the overlap weighting factors [15] $f_{\pi\pi} = 0.85$ (original value 0.585, adapted to excited singlet states of nitrogen heterocycles) and $f_{\sigma\sigma} = 1.00$ (1.267) to yield $\Delta E_{n\to\pi} = 2.66\,\text{eV} = 466\,\text{nm}$ for $E_x = 0$. This value equals the observed absorption wavelength of di-t-butyl nitric oxide (DTBNO) in a non-polar solvent (n-hexane) [23]. The calculated variation (blue shift) of $\Delta E_{n\to\pi}$ in the polarity range $0 \leq E_x \leq 0.01$ au amounts to 40 nm, which is close to the observed variation of 42 nm in a series of non-polar to polar solvents. This shows that $E_x \approx 0.01\text{au} = 5 \times 10^7\,\text{V cm}^{-1}$ is a reasonable estimate for the magnitude of the electric field in polar solvents (section 2.2).

The unpaired electron is distributed almost evenly over the NO bond (maximum variation approximately 10%) with the sum $\rho_\pi^N + \rho_\pi^O \cong 0.90 \pm 0.05$ being close to unity (figure 4). Thus roughly only 10% of ρ_π migrates into the adjacent five-membered hydrocarbon ring.

As anticipated by a simple picture, using the superposition of two canonical structures (non-polar and ionic) as proposed by Griffith *et al.* [11], ρ_π^O drops with increasing solvent polarity, accompanied by a comparable increase of ρ_π^N. The calculated variation of ρ_π^N in the range $0 \leqslant E_x \leqslant 0.02$ au is in accordance with the observed variation of A_{zz}^N by about 8%, i.e., $33.6 \leq A_{zz}^N \leqslant 37$ G, see figure 1.

The lone pair density c_{ny}^2 on the O atom decreases with increasing polarity due to an increase in c_y^2 on the N atom. The polarity dependence of the three quantities ρ_π^O, c_{ny}^2, and $\Delta E_{n\to\pi}$ acts on g_{xx} in the same direction: a lowering of g_{xx} with increasing polarity. This fact establishes the high sensitivity of this particular tensor component, g_{xx}, towards changes in polarity.

Hydrogen bonding also operates in the same direction as E_x on all three quantities ρ_π^O, c_{ny}^2, $\Delta E_{n\to\pi}$, thus leading to an additional lowering of g_{xx}. This has also been found by other authors, e.g., Un *et al.* [4] and Engström *et al.* [7]. Qualitatively, the calculated hb shifts shown in figure 4 (dashed lines) arise from an increasing admixture of the ionic electronic state (decrease of ρ_π^O), from the delocalization of the lone pair electrons into the H_2O orbitals (decrease of c_{ny}^2) and from a lowering of the energy of the lone pair orbital (increase of $\Delta E_{n\to\pi}$), respectively. Equivalent ZINDO/S calculations on the INDO-optimized structure of NO1 give very similar results as for the PM3 structure, with deviations $\leqslant 3\%$.

3.2.2. *Calculation of g_{xx} versus E_x without and with hydrogen bonding*

Figure 5 presents the calculated values of g_{xx} versus E_x using the rigorous methods G-RHF/S1 and G-RHF/S2, based on equations (2) and (3), and the approximate approach of equation (4) without and with hydrogen bond formation. The g_{xx} values of the rigorous

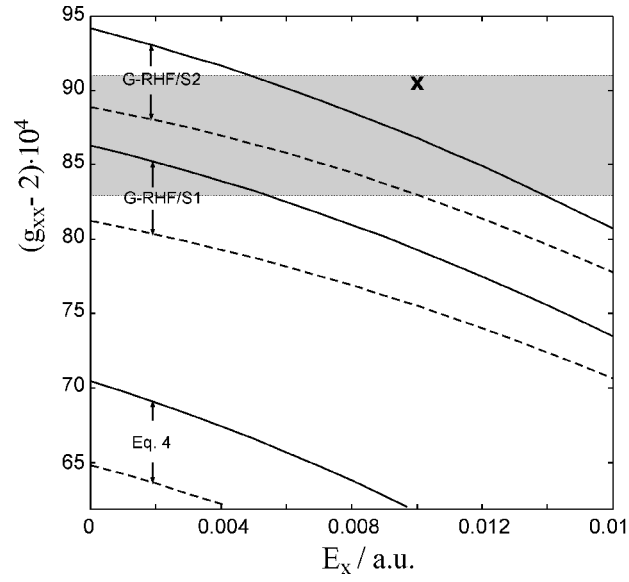

Figure 5. *g* tensor component g_{xx} versus E_x using methods G-RHF/S1, G-RHF/S2 and equation (4) without and with hydrogen bond formation (dashed lines). The point × stands for the G-RHF/S2 result in a strongly inhomogeneous field E_x without hydrogen bond formation (g_{xx} is shifted upwards by 3.6×10^{-4} from the corresponding homogeneous case, for details, see text). The shaded region indicates the full g_{xx} range covered by the MTS spin label in BR[1, 2], in the non-polar/aprotic solvent toluene/polystyrene and in water (figure 1).

G-RHF/S methods span the range 2.0070–2.0094 over the polarity region $0 \leqslant E_x \leqslant 0.016$ au. This encloses the variation $2.0083 \leqslant g_{xx} \leqslant 2.0091$ observed for the NO spin label MTS over the full polarity range (figure 1). However, the G-RHF/S1 method yields g_{xx} values systematically too small. In particular, if looking at the non-polar limit $E_x = 0$ (presumed point A in figure 1) where $g_{xx}(\text{obs}) \cong 2.0091$, we obtain $g_{xx}(\text{calc}) \cong 2.0086$ by the G-RHF/S1 method. By contrast, the G-RHF/S2 method produces an improved value of $g_{xx}(\text{calc}) \cong 2.0094$.

The use of equation (4), on the other hand, can serve as only a rough estimate for g_{xx}. The major deficiency of this approach comes from the neglect of the higher excitation states included in equation (3) and from the neglect of spin–orbit contributions from the nitrogen atom.

However, all three methods produce roughly the same slope $\mathrm{d}g_{xx}/\mathrm{d}E_x$ in the range $0 \leqslant E_x \leqslant 0.02$ au, since all curves differ only by nearly constant vertical shifts along the g_{xx} axis.

The calculated average slope $|\mathrm{d}g_{xx}/\mathrm{d}E_x| \cong 1.5 \times 10^{-11}\,\text{cm V}^{-1}$ is close to the corresponding experimental value $(2.0 \pm 0.3) \times 10^{-11}\,\text{cm V}^{-1}$ found in the study by Gullá *et al.* [9] (section 1). The latter value was also

ascertained theoretically in this same laboratory by a subsequent *ab initio* calculation [24] on the structurally similar nitroxide radical 2,2,5,5-tetramethyl-3,4-dehydropyrrolidine-1-oxyl (TMDP).

Hydrogen bond formation produces calculated g_{xx} shifts of about -4×10^{-4} in all three approaches. All three quantities, ρ_π^O, c_{ny}^2, and $\Delta E_{n\to\pi}$, contribute almost equally to this shift (5%, 4%, 3%, respectively). Interestingly, hydrogen bonding shows practically no effect on A_{zz}^N in our calculations because ρ_π^N remains almost unchanged (figure 4). The π spin density is mainly redistributed among the σ (p_x, p_y) orbitals on the O atom, since the PM3 structure of NO1 + H_2O is not strictly planar. The effects of hb on the g_{xx} versus A_{zz}^N dependence will be discussed in detail in the following section.

Strongly inhomogeneous electric fields from nearby charges can cause significant deviations from the homogeneous limit. For example, a positive charge of $+0.89e$ placed on the x axis at a distance of 5 Å from the O atom produces a highly inhomogeneous electric field of magnitude $E_x \cong 0.01$ au at the NO bond midpoint, and shifts g_{xx} by about 4×10^{-4} above the value for a homogeneous field of the same magnitude (see figure 5, point marked by ×, calculated by G-RHF/S2). However, since ρ_π^N is also affected, the consequences for g_{xx} versus A_{zz}^N are less pronounced (see below).

The calculations show g_{yy} to be practically independent of E_x with $g_{yy} - 2 = (40.4 \pm 0.1) \times 10^{-4}$ and $g_{yy} - 2 = (44.3 \pm 0.4) \times 10^{-4}$ for G-RHF/S1 and S2, respectively. The calculated hb shifts for this tensor component are of the order of $\Delta g_{yy} \cong -1 \times 10^{-4}$.

3.2.3. g_{xx} *versus* A_{zz}^N *for planar NO1*

In figure 6 we depict the calculated g_{xx} versus A_{zz}^N dependence for the planar NO1. In this plot we restrict ourselves to the G-RHF/S2 results because of the best quantitative agreement between calculated and experimental g_{xx} values at the non-polar limit $E_x = 0$. The conversion of E_x to A_{zz}^N on the abscissa is based on the relation $A_{zz}^N = Q_{tot}^N \rho_\pi^N$ for planar NO1, where $\rho_s^N = 0$ (equation (7)) and $Q_{tot}^N = 73$ G (equation (8)), and on the calculated, basically linear relationship $\rho_\pi^N = f(E_x)$ plotted in figure 4. The upper dashed line, defined as 'aprotic', is based on the calculated g_{xx} values without hydrogen bond formation. The lower dashed line is based on the calculated g_{xx} values with hydrogen bond formation. The solid line defined as 'protic' in analogy with the definition by Kawamura *et al.* [23] is derived by connecting the points A and B, characterized by the non-polar/aprotic limit with $A_{zz}^N = 33.6$ G and by the highly polar and protic condition in water with $A_{zz}^N = 36.4$ G, respectively. These two points, A and B, are the theoretical counterparts to the experimental limiting points A and B, respectively, in figure 1.

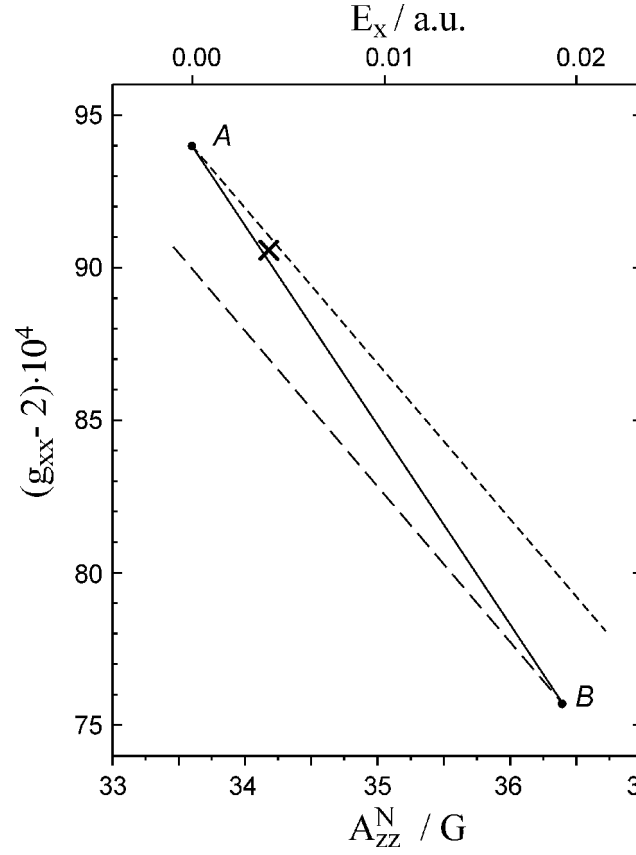

Figure 6. Plot of g_{xx} versus A_{zz}^N for planar NO1 as calculated by method G-RHF/S2 and by equation (7) with $\rho_s^N = 0$, for the aprotic case (without hydrogen bonding, short dashed) and with hydrogen bonding (long dashed). The 'protic' line (solid line) is obtained by linear interpolation between the non-polar limit (point A, $A_{zz}^N = 33.6$ G) and the water limit (point B, $A_{zz}^N = 36.4$ G), see text. Also shown is the calculated 'inhomogeneous' case marked by × (figure 5) and discussed in the text. All plotted curves have been linearized over the given range of A_{zz}^N. The g_{xx} shift of the line with hydrogen bonding against the aprotic line has been averaged to -4.0×10^{-4}.

Any point between the two limiting lines with (long-dashed) and without (short-dashed) hydrogen bonding can be assigned a fractional hydrogen bonding q_{prot} between 0 (point A) and 100% (point B) to serve as a measure of the protic interaction (proticity). In terms of the g_{xx} values at a particular polarity E_x (i.e. for $A_{zz}^N = \text{const}$) we thus define

$$q_{prot}(\%) = 100\{g_{xx} - g_{xx}(\text{aprotic})/\Delta g_{xx}(\text{hb}), \qquad (9)$$

where $\Delta g_{xx}(\text{hb})$ is the hydrogen bonding shift for the free NO spin label in H_2O and for setting $q_{prot}(H_2O) = 100\%$.

Our calculations yield $\Delta g_{xx}(\text{hb}) = -(4 \pm 1) \times 10^{-4}$ if we take its average value over the full polarity range $0 \leqslant E_x \leqslant 0.02$ au. According to the above definition,

the protic line is thus characterized by values of q_{prot} that are in direct proportion to the local electric field E_x:

$$q_{prot} = \text{const} \times E_x \qquad (\text{protic line}). \qquad (10)$$

Refering to the experimental results presented in figure 1, we have transferred the calculated shift $\Delta g_{xx}(\text{hb}) = -4 \times 10^{-4}$ into this plot, thus obtaining a graphical presentation entirely analogous to figure 6. Experimental verification of $\Delta g_{xx}(\text{hb})$ would require measurements of g_{xx} and A_{zz}^{N} for the MTS label in a model system characterized by a highly polar and aprotic microenvironment. Unfortunately, several attempts to achieve this goal failed. Details concerning this aspect are presented in the appendix. However, measurements of g_{iso} on a similar NO label in various solvents by Kawamura *et al.* [23] yielded $\Delta g_{iso}(\text{hb}) = -(2.0 \pm 0.5) \times 10^{-4}$. This gives $\Delta g_{xx}(\text{hb}) \cong 3\Delta g_{iso}(\text{hb}) = -(6 \pm 2) \times 10^{-4}$ which is compatible with our theoretical result.

Figure 1 shows that the majority of the spin label sites in BR are grouped closely around the protic line, thus demonstrating the close correlation between proticity and polarity in the protein. The triple mutant D96G/F171R1/F219L (point C) with $q_{prot} \cong 18\%$ reveals an almost non-polar and aprotic environment. This is explained by an opening of the proton entrance channel followed by a reorientation of the NO group towards a microenvironment of lower polarity and reduced hydrogen bonding accessibility. Spin labels at position 167 with $q_{prot} \cong 64\%$ instead of the regular 95% show a significant departure from the general proticity/polarity behaviour by revealing the stronger aprotic character of the cytoplasmic moiety of the proton channel, in spite of the high polarity of this region.

3.3. *The g_{xx} versus A_{zz}^{N} 'slope problem'*

The slopes of the calculated aprotic and protic lines are

$$(\mathrm{d}g_{xx}/\mathrm{d}A_{zz}^{N})_{aprotic} = -5.1 \times 10^{-4}\,\mathrm{G}^{-1}, \qquad (11a)$$

and

$$(\mathrm{d}g_{xx}/\mathrm{d}A_{zz}^{N})_{protic} = -6.5 \times 10^{-4}\,\mathrm{G}^{-1}. \qquad (11b)$$

These values are considerably larger in magnitude than the respective slopes $-1.1 \times 10^{-4}\,\mathrm{G}^{-1}$ and $-2.5 \times 10^{-4}\,\mathrm{G}^{-1}$ derived from the experimental results presented in figure 1. In previous studies, very different slope values have been found experimentally for different NO labels, e.g., (i) slopes of $-2.9 \times 10^{-4}\,\mathrm{G}^{-1}$ (aprotic), $-4.4 \times 10^{-4}\,\mathrm{G}^{-1}$ (protic) for di-t-butyl nitric oxide in liquids [23] and (ii) slopes varying by a factor of 10 between $-0.6 \times 10^{-4}\,\mathrm{G}^{-1}$ and $6 \times 10^{-4}\,\mathrm{G}^{-1}$ for phosphatidylcholine (PC) labels in phospholipid membranes [25]. In the latter study, it is speculated that sterically induced strains on the PC labels may influence the slopes $\mathrm{d}g_{xx}/\mathrm{d}A_{zz}^{N}$ observed.

We have considered structural changes of the NO label by the superimposed local electric field as a possible reason for the striking difference between the calculated and observed slopes $\mathrm{d}g_{xx}/\mathrm{d}A_{zz}^{N}$. Such structural changes are expected to occur especially in regions within the NO label possessing strongly inhomogeneous charge distributions (local electric dipole moments). This concerns mainly the NO bond itself but can also apply to the 'tail' of the label including the backbone atoms. Thus, structural changes may extend over the whole label structure, depending mainly on the 'stiffness' of the various torsional angles. A particularly sensitive structural parameter of this type is the angle φ between the NO bond and the plane of the attached 5-membered ring (see inset of figure 7). MO calculations show this angle to be a very 'soft' geometrical parameter, i.e., large changes in φ require only small changes in total energy. Specifically, the calculated change in total energy between the planar and the distorted cases for $\varphi = 20^{\circ}$ is only 0.005 au = 0.15 eV (INDO). This value increases only insignificantly when replacing the H atoms adjacent to the NO bond by CH_3 groups. This torsional energy is therefore significantly lower than the 'orientational' energy of the electric dipole of the NO bond in a polar environment. Using the calculated dipole moment of $\mu = 6\,\mathrm{D}$ and $E_x = 0.01$ au, this orientational (electrostatic) energy is $\mu E_x \cong 0.1$ au, so that only a small fraction of this energy is sufficient to strongly distort the spin label geometry.

Therefore we might expect that the polar environment, the electric vector **E** in our terms, induces changes in the angle φ. We term this situation 'polarity induced steric strain'. The functional relation $\varphi = \varphi(\mathbf{E})$ reflects a property of the entire label (including backbone atoms) but can, in special cases, also depend on external perturbations such as spatial restrictions due to interacting amino acid residues. Obviously we may exclude effects of the latter sort in the present study because of the observed linear g_{xx} versus A_{zz}^{N} relation. Such effects could, however, be responsible for the strongly varying slopes $\mathrm{d}g_{xx}/\mathrm{d}A_{zz}^{N}$ observed on PC labels in phospholipid membranes [24], see above.

We have been able to fit the calculated slope of the aprotic line to its experimental value by setting $\varphi = 24^{\circ}$ at $E_x = 0.01$ au. Table 1 shows that this structural change has two main effects: (1) an increase in g_{xx} caused by a significant lowering of $\Delta E_{n\to\pi^*}$ (this arises from a lowering of the orbital energy of the unpaired electron), and (2) an increase in A_{zz}^{N} caused by the contribution of $\rho_s^{N} \neq 0$ (equation 7), inspite of the

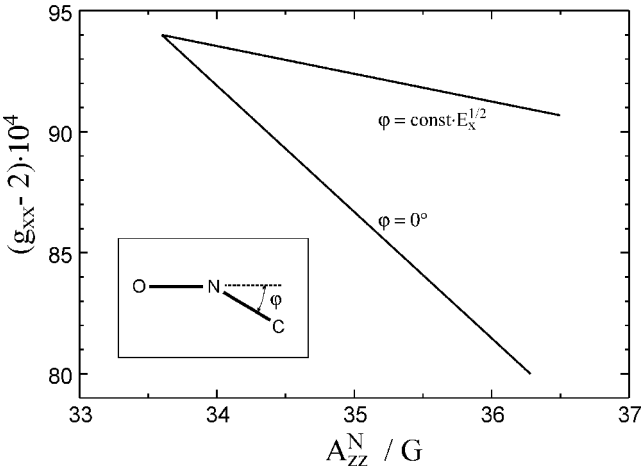

Figure 7. Variation of the slope of g_{xx} versus A^N_{zz} caused by deviations from planarity ('polarity induced steric strain'), see text. Aprotic case, PM3 geometry, and G-RHF/S2 method. Equation (7) was used to account for $\rho^N_s \neq 0$. The inset shows the structural parameter φ as the angle between the NO bond and the adjacent NCC plane.

considerable lowering of ρ^N_π. The combined action of these two effects leads to a significant decrease (in magnitude) of the slope dg_{xx}/dA^N_{zz} from $-5.1 \times 10^{-4}\,G^{-1}$ to $-1.1 \times 10^{-4}\,G^{-1}$, see table 1 and figure 7.

By fitting the calculated values of g_{xx} and A^N_{zz} for various values of φ and the electric field E_x to the observed straight line dependence of g_{xx} versus A^N_{zz}, we derived the empirical relation

$$\varphi = \text{const} \times E_x^{1/2} \qquad (12)$$

with the proportionality const $= 240^\circ\,\text{au}^{-1/2}$. Equation (12) expresses a linear correspondence between the dipole energy μE_x and the potential energy of the planarity restoring forces with a torsional harmonic potential $V_{pot} \propto \varphi^2$.

4. Conclusion

We have calculated polarity and hydrogen bonding effects on the g and hyperfine tensors of an NO spin label model by semiempirical molecular orbital methods. A comparison of theoretical and experimental results suggests that polarity effects may be described sufficiently well by a homogeneous electric field oriented along the NO bond, whereas hydrogen bonding effects may be realized by an energy minimized label/H_2O molecular pair model. Essentially, both types of effect may be traced to changes in the following molecular quantities: the π spin densities ρ^O_π and ρ^N_π, in special cases also ρ^N_s, the electron population of the $2p_y$ component of the oxygen lone pair orbital c^2_{ny}, and the $n \rightarrow \pi$ excitation energy $\Delta E_{n\rightarrow\pi}$. The combined action of polar and hydrogen bonding effects provides a semiquantitative understanding of g_{xx} versus A^N_{zz} for NO labels in different polar and protic microenvironments. This makes it possible to characterize semiquantitatively the hydrophobic barrier of the proton channel in bacteriorhodopsin by quantifying the accessibility of the respective protein region for water molecules. Structural strain indirectly imposed on the NO spin label by its polar environment and termed 'polarity induced structural strain' can severely affect the magnitude of the observed tensor components g_{xx} and A^N_{zz} by strongly reducing the slope dg_{xx}/dA^N_{zz} of linear plots of g_{xx} against A^N_{zz}. These phenomena may be rationalized by the assumption of bending forces leading to distortions from the planar structure of the NO label.

We gratefully acknowledge the support of the Deutsche Forschungsgemeinschaft in the frame of the Schwerpunkt-Programm SPP 1051 and the Sonderforschungsbereiche SFB 498 and SFB 533.

Appendix

In order to model a highly polar and aprotic environment, frozen solutions of 0.1–0.5 mM of MTS and of perdeutero-1-oxil-2,2,5,5-tetramethyl-Δ^3-pyroline-3-hydroxymethyl, which is structurally close to the NO1 model label, were investigated in the following solvents: (i) ethyl acetate ($\varepsilon_{293} = 6.0$, dipole moment 1.78 D), (ii) 1,2-propylene oxide (2.0 D), (iii) *N*,*N*-dimethylformamide ($\varepsilon_{293} = 37.0$, 3.8 D), (iv) sulpholane ($\varepsilon_{303} = 43.4$, 4.8 D), and (v) dimethyl sulphoxide ($\varepsilon_{293} = 46.7$, 3.9 D). These were purchased from Aldrich in their driest commercially available forms and, if necessary, were additionally dried using a molecular sieve (3 Å). Sulpholane and dimethyl sulphoxide were mixed in five different proportions to get a better glass. The W

Table 1. Effects of non-planarity on the slope dg_{xx}/dA^N_{zz} (assuming linearity of g_{xx} versus A^N_{zz}): aprotic case. Arrows ↑↓ indicate increase or decrease when φ changes from 0 to 24°. A^N_{zz} is calculated by equation (7) including effects from $\rho^N_s \neq 0$.

E_x/au	φ	ρ^N_π	ρ^N_s	$\Delta E_{n\rightarrow\pi}$/eV	$(g_{xx}-2)\times10^4$	A^N_{zz}/G	$(dg_{xx}/dA^N_{zz})/10^{-4}\,G^{-1}$
0.00	0	0.459	0.000	2.73	94.0	33.6	—
0.01	0	0.482	0.000	2.92	86.6	35.1	-5.1
0.01	24	0.449 ↓	0.014 ↑	2.75 ↓	91.3 ↑	36.0 ↑	-1.1 ↓

band EPR spectra were obtained at 120 K and evaluated as described previously [1]. Unfortunately, an analysis of the results obtained showed that in all the cases investigated the environment cannot be characterized as highly polar in terms of the present study. The highest value of A_{zz}^{N} in a sulpholane/dimethyl sulphoxide mixture of 90%/10% v/v does not exceed 34.5 G, with the corresponding g_{xx} value above 2.0088. All the measured points lie between A and C in figure 1. Thus, at present, we are not able to obtain an unambiguous verification of Δg_{xx}(hb) or to separate the effects of proticity and polarity in frozen solution.

Previous investigations of nitroxides in frozen solutions of other highly polar aprotic solvents (acetone ($\varepsilon_{293} = 21.0$, 2.88 D), methyl formate ($\varepsilon_{288} = 9.2$, 1.77 D) [8], and hexamethylphosphoramide ($\varepsilon_{293} = 31.3$, 5.4 D) [26]) also show quite small polarity effects on the nitroxide EPR parameters A_{zz}^{N} and g_{xx}.

All these results are in contrast to the following findings. 1, A high field EPR study showed a marked effect of the electrostatic microenvironment on the nitroxide g tensor when observing g values in pH adjusted solids [9]. 2, Previous theoretical investigations also predict significant polarity effects [7]. 3, Significant polarity effects are observed experimentally on isotropic A and g values in liquid solution [11, 23] and on g and A tensor components in a protein [1, 2] or in lipid environments [25].

Obviously, one needs to distinguish clearly between three situations: (a) liquid solution, (b) frozen solution, and (c) a protein-like environment, since these cases are expected to differ in their environmental averaging effects on the microscopic scale.

References

[1] Steinhoff, H.-J., Savitsky, A., Wegener, C., Pfeiffer, M., Plato, M., and Möbius, K., 2000, *Biochim. Biophys. Acta*, **1457,** 253.

[2] Wegener, C., Savitsky, A., Pfeiffer, M., Möbius, K., and Steinhoff, H.-J., 2001, *Appl. magn. Reson.*, **21,** 441.

[3] PM3 method: Stewart, J. J. P., 1989, *J. comput. Chem.*, **10,** 209, 221; INDO method: Pople, J., and Beveridge, D. L., 1970, *Approximate Molecular Orbital Theory* (New York: McGraw-Hill); ZINDO/S method: see [15].

[4] Un, S., Atta, M., Fontecave, M., and Rutherford, A. W., 1995, *J. Amer. chem. Soc.*, **117,** 10713.

[5] Törring, J. T., Un, S., Knüpling, M., Plato, M., and Möbius, K., 1997, *J. chem. Phys*, **107,** 3905.

[6] Knüpling, M., Törring, J. T., and Un, S., 1997, *Chem. Phys.*, **219,** 291.

[7] Engström, M., Owenius, R., and Vahtras, O., 2001, *Chem. Phys. Lett.*, **338,** 407.

[8] Owenius, R., Engström, M., Lindgren, M., and Huber, M., 2001, *J. phys. Chem.* A, **105,** 10967.

[9] Gullá, A. F., and Budil, D. E., 2001, *J. phys. Chem.* B, **105,** 8056.

[10] Lajzerowicz-Bonneteau, J., 1976, *Spin Labeling: Theory and Applications*, edited by L. J. Berliner (New York: Academic Press) p. 239.

[11] Griffith, O. H., Dehlinger, P. J., and Van, S. P., 1974, *J. Membrane Biol.*, **15,** 159.

[12] Stewart, J. J. P., 1989, *J. comput. Chem.*, **10,** 221.

[13] Stone, A. J., 1963, *Proc. R. Soc. Lond.* A, **271,** 424.

[14] Törring, J. T., 1996, Ph.D. thesis, Freie Universität Berlin.

[15] Ridley, J., and Zerner, M. C., 1973, *Theoret. Chim. Acta*, **32,** 111.

[16] Hsiao, Y., and Zerner, M. C., 1999, *Intl. J. Quantum Chem.*, **75,** 577.

[17] Carrington, A., and McLachlan, A. D., 1969, *Introduction to Magnetic Resonance* (New York: Harper and Row).

[18] Burghaus, O., Plato, M., Rohrer, M., Möbius, K., MacMillan, F., and Lubitz, W., 1993, *J. phys. Chem.*, **97,** 7639.

[19] Lemaire, H., and Rassat, A., 1964, *J. chim. Phys.*, **61,** 1580.

[20] Beveridge, D. L., and McIver Jr., J. W., 1971, *J. chem. Phys.*, **54,** 4681.

[21] Plato, M., Möbius, K., and Lubitz, W., 1991, *Chlorophylls*, edited by H. Scheer (Boca Raton, FL: CRC Press) p. 1015.

[22] Jeffrey, G. A., 1997, *An Introduction to Hydrogen Bonding* (Oxford University Press).

[23] Kawamura, T., Matsunami, S., and Yonezawa, T., 1967, *Bull. chem. Soc. Jap.*, **40,** 1111.

[24] Ding, Z., Gullá, A. F., and Budil, D. E., 2001, *J. chem. Phys.*, **115,** 10685.

[25] Earle, K. A., Moscicki, J. K., Ge, M., Budil, D. E., and Freed, J. H., 1994, *Biophys. J.*, **66,** 1213.

[26] Lebedev, Ya. S., Gringerg, O. Ya., Dubinsky, A. A., and Poluektov, O. G., 1992., *Bioactive Spin Labels*, edited by R. I. Zhadanov (Berlin: Springer-Verlag) p. 228.